Journal of Medical and Biological Engineering (2019) 39:470–479
https://doi.org/10.1007/s40846-018-0419-5

ORIGINAL ARTICLE

Experimental Research on the Impact of Alveolar Morphology on Deposition of Inhalable Particles in the Human Pulmonary Acinar Area

Rong Li[1,2] · Xin-Xi Xu[1] · Yang Qiao[1] · Xiu-Guo Zhao[1]

Received: 23 November 2017 / Accepted: 2 May 2018 / Published online: 26 June 2018

Abstract
Studying the deposition pattern of inhalable particles in the pulmonary acinus has significance in clarifying the predisposing cause, progression, clinical treatment and prevention of common respiratory system diseases such as emphysema. In this study, we established an in vitro experimental model capable of simulating pulmonary acinar morphological lesions, such as emphysema and pulmonary atrophy. In addition, the deposition efficiencies of inhalable particles with various diameters in the pulmonary acinus were investigated under an unsteady state respiratory mode. The changes in pulmonary acinar morphology significantly affected the deposition rates of particles. Moreover, alveolar atrophy increased the deposition rate of particles, while pulmonary alveolar dilatation decreased the deposition rate. The results of this study may provide experimental evidence for the development of a disease course by pulmonary acinus morphologic changes. The established model also provides a feasible in vitro experimental model for studying the deposition pattern of inhalable particles in the pulmonary acinus.

Keywords Pulmonary acinus · Inhalable particles · Deposition · Alveolar morphology

1 Introduction

With the acceleration of global industrialization, air pollution has resulted in the common occurrence of respiratory disease. In particular, the deposition of inhalable particles (airborne particles with an aerodynamic diameter ≤ 10 μm) in the lung is the major predisposing cause of respiratory diseases. The pulmonary acinar area is the major functional area of the human respiration system. The deposition of inhalable particles in the pulmonary acinus can cause pulmonary lesions and affect pulmonary functions. Inhalable particles can further penetrate the alveolar walls to enter the human blood circulatory system, causing substantial damage to human health. Therefore, studies of the deposition patterns of inhalable particles in the pulmonary acinus area have significance for understanding the etiology, treatment, and prevention of emphysema and other diseases.

Presently, studying acinar deposition by subjecting human subjects to direct inhalation of particles has substantial potential health risks and high costs. Moreover, due to the complex structure and small size of the pulmonary acinus, it is impossible to establish a life-size computer model or physical model through Computed Tomography (CT) scanning. Therefore, most studies have used theoretical models, simplified empirical models or simplified physical models to perform computerized simulation analysis or experimental research. Some investigators have established two-dimensional or three-dimensional single-level or multiple-level computer models of the pulmonary acinus to study the respiratory flowfield and deposition distribution of particles with various diameters [1–3]. These researchers determined that the respiratory flowfield in pulmonary alveoli exhibited oscillatory laminar flow and formed a partial vortex in the respiratory transition. Darquenne et al. [4] showed that gravity had an important impact on the deposition of fine particles, and the deposition of particles in various levels of the alveolar ducts was heterogeneous. In addition, they found

✉ Xin-Xi Xu
xuxx1@sohu.com

[1] Institute of Medical Support Technology, Academy of Military Sciences, Tianjin 300161, China

[2] Department of Military Protective Medicine Logistics, University of Chinese People's Armed Police Force, Tianjin 300309, China

that particles with diameters less than 0.2 μm were mainly deposited in alveolar areas; therefore, they hypothesized that the deposition of particles in the pulmonary acinar area primarily relied on Brownian motion. However, the deposition of particles in the alveolar region is the result of coupling between convection and diffusion mechanisms [5]. Sznitman et al. [6] showed that the convection phenomena induced by alveolar wall movement inside alveoli played an important role in the deposition of particles in the pulmonary acinus. Ma et al. [7] established a continuous, asymmetric, five-generation, three-dimensional pulmonary acinar model with moving walls and found that moving walls and multiple breathing cycles had a substantial influence on the accurate deposition of particles in the pulmonary acinus. In recent years, some scholars have tried to simulate alveolar pathology abnormalities. Oakes et al. [8] established a computer model of a single cluster of healthy and emphysema pulmonary acinus and a particle image velocimetry (PIV) experimental model; the particle deposition efficiency in healthy alveoli was higher than that in emphysema alveoli. Li [9] studied the effect of small airway obstruction on the deposition of alveolar particles and found that bronchial obstruction would significantly reduce the deposition of particles in alveoli. These results are based on the hypothesis of the isotropic expansion of alveoli. However, Hofemeier et al. believe that pulmonary alveolar deformation is anisotropic because of lung breathing, which is not a regular circle. Hofemeier's computer simulation study showed that movement and deposition of submicron particles were significantly affected by changes in the anisotropy of alveoli [10]. However, in a subsequent study, Hofemeier et al. showed that alveolar anisotropy played only a secondary role in the impact of alveolar deposition at all levels [5]. Therefore, the effect of the anisotropy of alveoli on the deposition of particles needs further study.

Simultaneously, in vitro experimental models for the deposition of inhalable particles in the acinus must be established to compete with or confirm computer simulation results. Chhabra et al. [11] established a single elastic alveolar model and applied PIV to observe the flow-field distribution and deposition of inhalable particles in alveoli under an unsteady respiratory model. The results showed that a periodically changing vortex flowfield was present in alveoli, with the deposition efficiency changing dramatically from 0.1 to 10%. Berg et al. [12] established a planar model of a single acinar cluster with anatomical casting technology based on the lungs of healthy adult sand used PIV for flow-field analysis. In a single respiratory cycle, the particles could not directly reach the wall of alveoli; therefore, the deposition of particles in alveoli may be the result of the superposition of multiple respiratory cycles.

In the scaled model, PIV can be used to analyze only the motion of particles in the model. There are some problems in calculating the deposition rate of particles on the surface of the body by PIV. For example, when the deposition rate of a three dimensional (3D) surface is calculated, the PIV image will overlap and reduce measurement precision. Recently, researchers have tried to establish a life-size alveolar model to further reveal the movement and deposition of particles in alveoli. Fishler et al. has built many kinds of true-scale pulmonary acinar models based on microfluidic technology [13–15]. These models are characterized by thickness on the micron scale, and the whole model resembles the two-dimensional (2D) structure. Therefore, they used the PIV time-sharing imaging method to analyze movement and deposition of particles in alveoli during the respiratory cycle. This model overcomes the insufficiency of the dynamic similarity in the scaled models; nevertheless, the structure of the pulmonary acinus is too simplified. Therefore, the scaled model has some advantages in simulating the complex structure of the pulmonary acinus.

Current research on experimental models uses fluids such as glycerol to substitute air as the vector of particles. In addition, a few studies have described experimental models of the pulmonary acinus with pathological characteristics. In this paper, through establishment of a pulmonary acinar experimental model, we studied the deposition efficiencies of particles with various diameters in the terminal bronchioles and pulmonary acinar area, as well as the influence on deposition efficiency under an unsteady respiration mode. The results may reveal the relationship between the deposition of particles and pneumoconiosis, emphysema and other respiratory diseases and provide an experimental basis for disease prevention and treatment.

2 Experimental Model

2.1 Human Pulmonary Acinar Experimental Model

According to the human lung regions illustrated by the International Commission on Radiological Protection (International Commission on Radiological Protection, ICRP, 1994) [16], the 15th and 16th levels of bronchi are defined as terminal bronchioles, and the levels ≥ 17th are defined as the pulmonary acinar area. As shown in Fig. 1, the experimental model in this paper was designed as one segment of the 15th level bronchus, 2 segments of the 16th level bronchus and 4 segments of the pulmonary acinar area, with each pulmonary acinus containing 17 alveoli. The diameters, lengths and branching angles of the 15th–17th levels of the bronchioles and alveolar ducts all came from the Beatrice anatomical values [17] and were scaled 75 times. A demountable structure was placed in the middle of the bronchioles of each level to enable convenient placement of normal and pathological segments. During the deposition experiment,

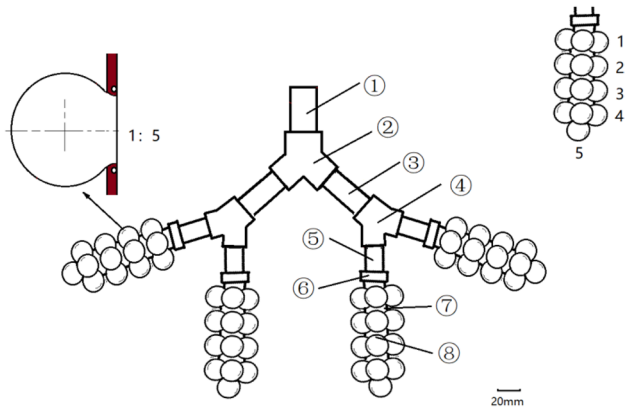

Fig. 1 Human pulmonary acinus experimental model. ① 15th-level bronchus; ② Connector; ③ 16th level bronchus; ④ Connector; ⑤ 17th level bronchus; ⑥ Connector; ⑦ Pulmonary alveolar duct; ⑧ Pulmonary alveolus

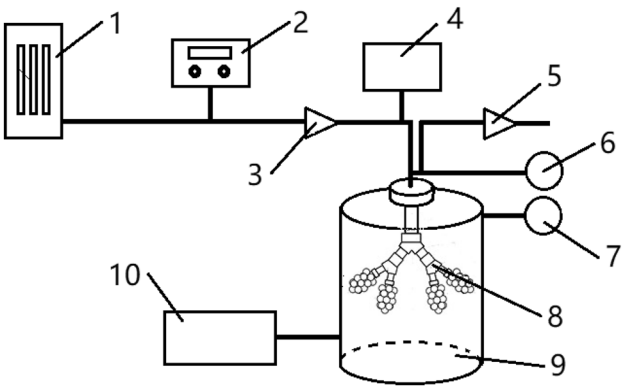

Fig. 2 Experimental model of deposition of inhalable particles in the human pulmonary acinus area. 1. Aerosol generator; 2. Laser particle counter; 3. Check valve; 4. Humidifier; 5. Check valve; 6. Humidity sensor; 7. Differential pressure sensor; 8. Human pulmonary acinus model; 9. Airtight test chamber; 10. Respiratory simulator

these segments could be removed to analyze the deposited particle concentrations.

The actual average diameter of a healthy adult alveolus is approximately 250 μm, with a wall thickness $\delta = 1.11$ μm, density 250 kg/m^3, Young's modulus E = 5 kPa and Poisson's ratio $\upsilon = 0.4$ [18]. After equivalent scaling, the diameter of the alveolus was 18.75 mm. The alveolar test model was made into a sphere, and the opening is round, with a circular fixing ring that could fix the pulmonary test model on the end of the bronchioles. Methyl vinyl silicone rubber is the basic material comprising the alveolar wall. By adding cyclic polymethylsiloxane as the softening agent, the moduli of Young's modulus are 5200 Pa, and Poisson's ratio is 0.43. The pulmonary alveolus of the test model can be removed and eluted to analyze the concentration of the deposited particles to measure deposition in the pulmonary alveoli alone. This model can be used for experimental analysis of particle movement and deposition in the pulmonary acinar area under various respiratory and environmental humidity conditions, including local and total deposition efficiencies and the effects of various lesions and particle diameters. The established model contains the 15th–17th bronchi and 4 acinar areas, and the total volume is 1772 mL. In addition, a separate alveolus with a 40% reduction of diameter is created as the pulmonary acinar model of patients with lung atrophy, and an alveolus with a 40% increase in diameter is created as the pulmonary acinar model of patients with emphysema; their diameters are 11.25 and 26.25 mm, respectively.

2.2 Experimental Model of Deposition of Inhalable Particles in the Human Pulmonary Acinar Area

As shown in Fig. 2, the inhalable particles used for the human pulmonary acinar area deposition experimental model are generated by an aerosol generator to produce monodispersed polystyrene microspheres. At the inlet of the model, a laser particle counter is used to measure the concentrations of the particles. After passing through the check valve, the microspheres enter the pulmonary acinar experimental model. A respiration simulation pump is used to introduce negative pressure inside the transparent test chamber to enable expansion of the alveoli of the pulmonary acinar experimental model, and the particle aerosol will be inhaled into the alveoli. After deposition, the respiration simulation pump creates positive pressure in the transparent test chamber in order to contract the alveoli, and the aerosol inside the pulmonary acinus will be discharged from the model through a check exhaust valve. When the device is in operation, a humidifier is used to adjust and simulate pulmonary acinar area humidity during respiration.

2.3 Respiration Mode

Oakes et al. [8] measured the flow curve of the unsteady slow breathing of a 21-year-old healthy man; it was approximately a sinusoidal curve. Therefore, in this study, we used a respiratory simulator to simulate the respiration mode, and the respiratory state is described as an unsteady sine function (Fig. 3).The exhalation and inhalation ratio is 1:1, the respiration frequency is adjustable, and the alveolar functional residual capacity is adjustable between 20 and 80%. Under the normal respiration mode, the alveolar functional residual capacity is set at 70%, i.e., the maximal alveolar deformation rate is 30%.

2.4 Experimental Model Hydrodynamics and Particle Transport Similarity

The experimental model dynamic similarity includes the similarity of the Reynolds number *Re* and Womersley

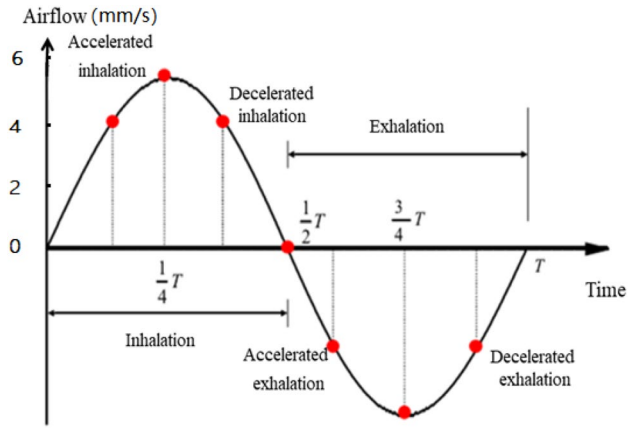

Fig. 3 Unsteady state respiratory cycle in the model

number *Wo* in the model. During respiration, the airflow in the bronchioles and pulmonary acinar area is a laminar flow in a steady state [19], with a Reynolds number Re < 1, and a *Wo* < 1. This experimental model is an equivalent amplification of the actual size of this area. According to the Reynolds number calculation formula $\mathrm{Re} = 8EV_i\omega/D\upsilon$ [8], *E* is the current expansion rate of alveoli, V_i is the total volume of alveoli, ω is the respiratory frequency, *D* is the diameter of the alveolar, and υ is the aerodynamic viscosity coefficient. Since the inhalation process of the human body is a humidification process of the air inside the respiratory tract, when the air reaches the alveoli, the humidity has been increased to 100%. Therefore, the air flow in the pulmonary acinus can be considered high-humidity, diluted two-phase flow, and its viscosity calculation can be obtained according to the calculation formula provided by the references [20, 21]; the measured value of the aerodynamic viscosity coefficient is $\upsilon = 13.26$ μPa s. The respiration cycle of the model is T = 4 s; therefore, when the maximal expansion rate is 70%, the alveolar Reynolds number Re = 0.06 < 1. According to the Womersley number calculation formula [8], *Wo* = 0.79 < 1.

Another important aspect of experimental model similarity is the similarity of particle motion, which depends on Stokes numbers (*Stk*), gravity number (*H*), and particle Peclet number (Pe_p). According to Sznitman et al. [22] and Hofemeier et al. [23], $Stk = \omega d_p^2 \rho_p C_c / 18\mu$. d_p is the diameter of the particles, $\rho_p = 1.05$ g/cm^3. The parameter C_c corresponds to the Cunningham slip correction factor. For all particle diameters considered, we note that $Stk \ll 1$ (see Table 1) such that aerosol deposition via inertial impaction is negligible in the acinus. $H = g d_p^2 \rho_p C_c / 9\mu D\omega$, D is the diameter of the alveoli. *H* may be interpreted as a parameter proportional to the ratio between the time scale for oscillatory flow (i.e., breathing period) and the characteristic gravitational sedimentation time. In our model, $H \ll 1$(see Table 1); thus, the particle deposition may be very slightly affected by sedimentation.$Pe_p = D^2\omega / D_{mol}$, and $D_{mol} = kTC_c / 3\pi\mu d_p$,where *k* is the Stefan–Boltzmann constant ($k = 1.38 \times 10^{-23}$ J/K), and T is the absolute temperature in Kelvins. Pe_p of different particle sizes are shown in Table 1, $Pe_p \gg 1$.

3 Materials and Methods

3.1 Materials and Equipment

In this paper, fluorescent polystyrene microspheres (Beijing HyperCyte Biomedical Co., Ltd.) are used as inhalable particles, including 0.1, 0.3, 1, 3 and 5 μm specifications.

An F9631 standard particle generator (Shenyang Xinke Precision Instrument & Equipment Co., Ltd., Shenyang, China) is used to produce a monodispersed polystyrene fluorescence microsphere aerosol. A respiratory simulator (Beijing HanwenWangxing Technology Co., Ltd., Beijing, China) is used to simulate various respiratory conditions. A YADU SC-D052AE humidifier (YADU Int'l Technology (Beijing) Co., Ltd., China) is used to humidify the chamber of the experimental model. A MP100 differential pressure sensor (KIMO Instruments, France) is used to monitor the pressure of the pulmonary acinus. A TSI8386 Velocicalc Plus Multi-Parameter Ventilation Meter (TSI USA) is used to monitor the relative humidity and temperature inside the pulmonary acinus. A TSI AeroTrak9350 Portable Particle Counter (TSI USA)is used to monitor the concentration of inhalable particles with diameters of 0.3–5 μm inside the experimental model. A Lasair II laser particle counter (PMS USA) is used to monitor the concentration of inhalable particles with a diameter of 0.1 μm inside the experimental model. An Attune NxT flow cytometer (Invitrogen ThermoFisher, USA) is used to count the number of deposited particles.

Table 1 Characteristic values of the dimensionless particle numbers across the range of particle sizes investigated under oscillatory acinar flow conditions

	d_p					
	0.1 μm	0.3 μm	0.5 μm	1 μm	3 μm	5 μm
Stk	1.94×10^{-6}	2.91×10^{-6}	1.21×10^{-5}	4.85×10^{-5}	4.36×10^{-4}	1.21×10^{-3}
H	1.1×10^{-4}	1.65×10^{-4}	6.86×10^{-4}	2.75×10^{-3}	2.47×10^{-2}	6.86×10^{-2}
Pe_p	9.56×10^{1}	1.07×10^{2}	1.19×10^{2}	1.19×10^{2}	7.17×10^{2}	1.19×10^{3}

3.2 Methods

3.2.1 Generation of Monodispersed Polystyrene Fluorescence Microsphere Aerosol

The stock solution of monodispersed polystyrene fluorescence microspheresis diluted to make the aerosol generation solution, with a concentration of 1×10^7 to 1×10^9/mL, which is placed into a F9631 standard particle generation device to generate a monodispersed aerosol with a generation flow rate of 80 L/min. Under this condition, the concentration generated by the F9631 standard particle generation device is 1×10^3 to 3×10^5/L. The concentration of the generation solution of larger diameter microspheres is relatively lower; therefore, the concentration of the generated aerosol is also lower.

3.2.2 Deposition of Inhalable Particles in the Pulmonary Acinus

The bronchioles of every level, connectors and pulmonary alveoli are washed by immersion in deionized water in an ultrasonic cleaner for 5 min. Then, the bronchioles, connectors and pulmonary alveoli are placed in a low-temperature desiccator to dry adequately and assembled on an ultraclean bench. The assembled structure is placed in an airtight experimental chamber and fixed. After the tubes and the sensors are connected, the air tightness of the experimental model is checked. The respiratory simulator is adjusted to the required respiration frequency, flow rate and functional residual capacity; the humidifier is adjusted to the preset value. The aerosol generator and particle counter are turned on to start the deposition experiment. Every 5 min during the experiment, the laser particle counter is used to record the concentration of the generated aerosol.

3.2.3 Counting Particle Deposition

In the test, the deposited particles in the deposition model are washed with washing buffer, and the number of deposited particles is counted in a flow cytometer. The flow cytometer can distinguish fluorescent particles from non-fluorescent particles; therefore, it can maximally reduce the interference of the amount of deposition by non-fluorescent particles. After the deposition experiment is completed, the pulmonary acinar model is removed and disassembled. The alveolus is soaked in 5 mL of deionized water for 1 h and shaken for 1 min on a vortex mixer. The bronchioles and alveolar ducts are placed in a test tube, 20 mL of deionized water is added to the tube, and the tube is shaken on a vortex mixer for 1 min. The solution is transferred to an EP tube with a pipette. The flow cytometer is used to measure the concentration of the particles; a 50 µL sample is injected each time at an injection rate of 12.5 µL/min.

3.2.4 Deposition Test Mode

We mainly observe the deposition efficiencies of particles with diameters of 0.1, 0.3, 1, 3 and 5 µm in the human pulmonary acinar experimental model. The deposition experiment modes include the following: (A) healthy alveoli, 30% expansion rate; (B) simulation of pulmonary atrophy lesion, 40% alveolar atrophy and 30% expansion rate; (C) 1 cluster of the 4 clusters of alveoli in the model had 40% alveolar atrophy, the rest were normal, 30% expansion rate; (D) simulation of emphysema lesions, 40% alveolar expansion and 30% expansion rate; and (E) 1 cluster of the 4 clusters of alveoli in the model had 40% expansion, 30% expansion rate. The respiration cycle is T = 4 s, the test time is 3–5 h, and the relative humidity in the alveoli is near 100%. Each mode is repeated 5 times.

3.2.5 Calculation of Deposition Efficiency

Formula 1 is used to calculate the deposition efficiency in bronchioles and alveoli.

$$DF_{\mathrm{i}} = \frac{N_{\mathrm{i}}}{V_{\mathrm{i}}(1-\delta)C_1}\times 100\% \tag{1}$$

where DF_i is the deposition efficiency of the ith level of bronchus or alveolus, N_i is the amount of particle deposition obtained by flow cytometer counting, and V_i is the actual total volume of the aerosol passing through the ith level of bronchioles and alveoli. Using the 15th level of bronchioles as an example, its actual total volume V_{15} is the sum of the volume of itself and the volume of bronchioles, alveolar ducts and alveoli. C_1 is the aerosol concentration of inhalable particles, which is represented by the average value of collected data in the test. δ is the residual respiratory rate.

4 Results and Discussion

4.1 Particle Deposition in a Healthy Pulmonary Acinar Area

The particle deposition results in the healthy pulmonary acinus deposition model (Model A) are shown in Figs. 4 and 5. For the 15th–17th bronchi at the front of the pulmonary acinus, the deposition efficiencies of particles with the same diameter were primarily the same, suggesting that the size and physiological environment of bronchioles were similar and that the hydrodynamic characteristics of

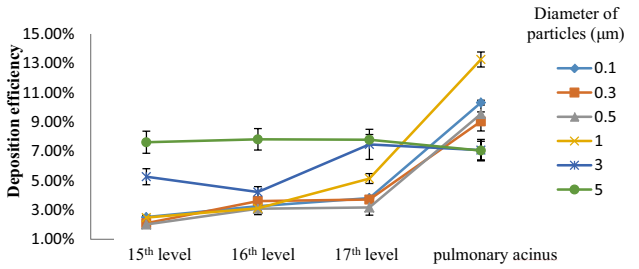

Fig. 4 Particle deposition results of healthy alveoli (Model A)

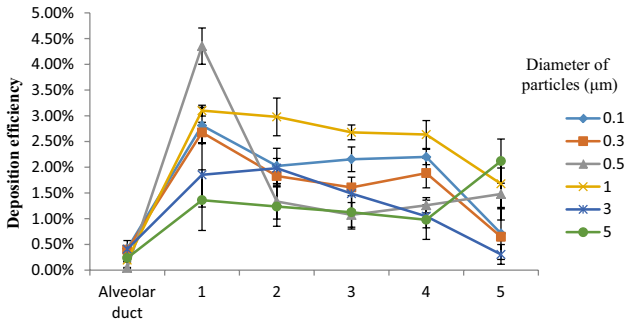

Fig. 5 Particle deposition results in the pulmonary acinus area in a healthy alveolar model (Model A)

the particles in bronchioles were also similar. The total deposition efficiencies of particles with diameters of 0.1–1 μm in the pulmonary acinus area were significantly higher than those in the proximal bronchus. For example, the total deposition efficiency of particles with a diameter of 0.1 μm in the pulmonary acinus area was 10.32%, which was similar to the simulation result (a pulmonary acinus deposition efficiency of 8.3%) in the literature [8], and was also consistent with the deposition result (10%) of a single alveolar experimental model after 20 cycles of respiration in the literature [9]. The particles with a diameter of 1 μm had the highest deposition efficiency (13.27%) in the pulmonary acinar area, followed by those with diameters of 0.1 μm, while particles with diameters of 3–5 μm had the lowest deposition efficiencies in the pulmonary acinar area. A previous report [1] showed that prior to the deposition of particles on the alveolar wall, the particles would enter a long period of vortex circulation instead of flowing out of the alveoli with the exhalation process. In a reported model [24], the particle deposition efficiency was increased with the increase in there spiration cycle number. These experimental results were consistent with results in this paper; specifically, under the balance of the inertia effect and Brownian motion, 1 μm particles had the longest suspension time in alveoli. Over time, their probability to reach the alveolar wall and deposit was the highest.

As shown in Fig. 5, the deposition efficiencies of different areas of the pulmonary acinus varied slightly. As a common pathway of multiple alveoli, the inner surface area of the alveolar duct was very small; thus, the deposition efficiency was generally lower than 0.5%. There was no significant change in the deposition efficiency in the 1–4 levels of alveoli, suggesting that the deposition change of particles in the pulmonary acinus was relatively even. A single cluster of the pulmonary acinus could be considered the basic unit of respiration and could be considered a whole in future studies [25]. The previously established PIV experimental model showed that very few airflow lines could reach the terminal alveoli of the pulmonary acinus and that the flow rate was extremely slow. In the experimental model of this paper, the decrease in the deposition efficiency at the terminus of the pulmonary acinus (i.e., the 5th level of alveoli) was significant, which adequately suggested that particle flow lines rarely reach the terminal alveoli for healthy alveoli under the normal respiration mode.

4.2 Effect of Alveolar Atrophy or Local Atrophy on Particle Deposition in the Pulmonary Acinar Area

When pneumoconiosis, tuberculosis, alveolar fibrosis and other lesions occur, alveoli undergo various degrees of atrophy. In our experimental model, alveolar atrophy was divided into two forms; in one, all alveoli in the model had 40% atrophy (Model B), while in the other, alveoli in region I had 40% atrophy, and the rest were healthy (Model C). The test results of the deposition efficiencies of particles with various diameters in these two models are shown in Figs. 6, 7 and 8. In Model B, the deposition trend of particles with various diameters in the bronchi and pulmonary acinus were essentially consistent with that of particles in healthy alveoli. There was a slight difference because the atrophy of alveoli

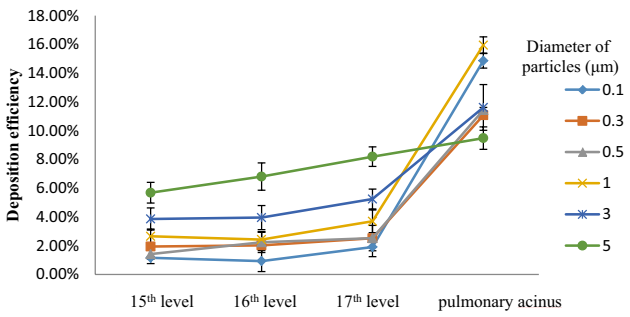

Fig. 6 Particle deposition results when alveoli decrease in size (Model B)

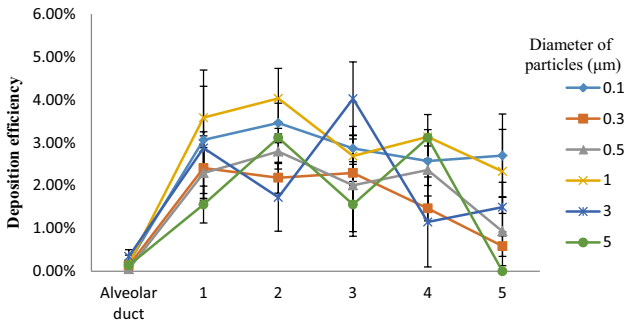

Fig. 7 Results of particle deposition in the pulmonary acinus area when alveoli decrease in size (Model B)

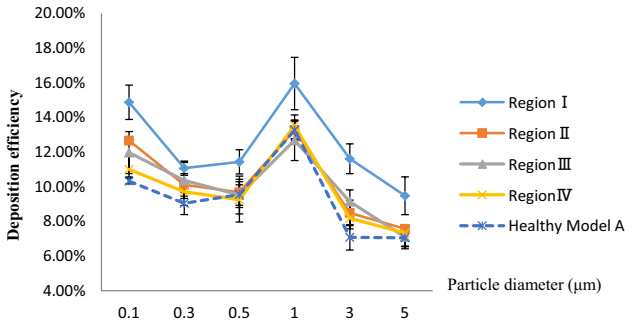

Fig. 8 Particle deposition results when alveoli decrease in size locally (Model C)

caused a rather consistent increasing trend of particle deposition efficiency in the 15th level bronchus of the pulmonary acinus. The total deposition efficiency of atrophic alveoli in the pulmonary acinar area was significantly higher than that of healthy alveoli, whereas the deposition efficiency in the 15th–17th level bronchi were slightly lower than that in the healthy model (Model A). Based on analysis from the hydrodynamics perspective, after alveoli atrophy, the degree of vortex in alveoli was decreased; thus, the flow line was more similar to a laminar flow, causing the particles to more easily reach the alveolar wall, and the deposition efficiency was increased. The respiration process was a reciprocating process; the increase in the deposition efficiencies of particles in the pulmonary acinus would inevitably result in a decrease of particle deposition efficiency in its proximal bronchus. Medical studies have shown that the development of pneumoconiosis is an accelerated process [26]; the major reason for this accelerated process might be that alveolar atrophy caused the deposition efficiency of particles to increase. The particle deposition efficiency in the same cluster of the atrophic pulmonary acinus did not vary greatly, but it was not as even as that in healthy alveoli, suggesting that the unsteady state of the respiratory process after alveolar atrophy was exacerbated. In addition, the increase in the deposition efficiency of particles with smaller diameter in atrophic pulmonary acinus was larger; the major reason for this increase might be that fine particles could more easily reach the alveolar wall in the laminar flow. When particles are smaller in diameter, it is easier for particles to reach the alveoli. Therefore, promotion of deposition of fine particles in alveoli by alveolar atrophy might cause pneumoconiosis and tuberculosis, further reducing their resistance to polluted air.

In Model C, the deposition efficiencies of the particles of atrophied alveoli in region I did not significantly differ from the test results in Model B. The deposition efficiencies of particles in other regions were slightly higher than those in the completely healthy Model A. However, there was no study to confirm that such a slight difference was caused by the change in region I. Whether the increase in particle deposition efficiency caused by certain clusters of atrophic alveoli could promote particle deposition in the adjacent alveoli requires studies with longer term respiration processes for verification.

4.3 Effects of Alveolar Expansion or Local Expansion on Particle Deposition in the Pulmonary Acinar Area

From the medical perspective, the factors that cause emphysema mainly include bronchial obstruction and the imbalance of alveolar elastase and its inhibitor [20]; the direct impact is the volume increase in the associated alveoli. Models D and E established lesion models for a multiple-cluster pulmonary acinar volume increase and a single-cluster pulmonary acinar volume increase, respectively. As shown in Table 2, after alveolar expansion (Model D), the deposition efficiency of particles in the pulmonary acinar area significantly decreased ($p < 0.01$). However, the deposition efficiency in the adjacent bronchiole region increased. Figure 9 shows the experimental result of a local emphysema model (Model E). The particle deposition efficiency in the emphysema region (region I) was significantly lower than that in other healthy areas, whereas there were no significant differences between the deposition efficiencies in other regions and that in a complete healthy alveolar model (Model A). Oakes et al. [26] used a computer model to study the alveolar expansion caused by emphysema and reached a conclusion consistent with this study. Since the Stokes number is very small, the effect of inertial collision deposition is not significant. The enlargement of the alveoli increases the difficulty diffusion of the particles to the alveolar wall; thus, the deposition rate is reduced. Another study [8] used PIV

Table 2 Comparison of particle deposition efficiencies (%) in alveolar expansion (Model D) and healthy alveoli

Particle diameter	0.1		0.3		0.5		1.0		3.0		5.0	
	Healthyalveoli	Expansion alveoli	Healthy alveoli	Expansion alveoli	Healthy alveoli	Expansion alveoli	Healthy alveoli	Expansion alveoli	Healthy alveoli	Expansion alveoli	Healthy alveoli	Expansion alveoli
15th level	2.52	2.71	2.10	2.86	2.02	2.53	2.48	2.82	5.27	6.35	7.62	8.35
16th level	3.26	4.65	3.61	4.04	3.09	3.89	3.12	3.73	4.22	4.75	7.82	7.77
17th level	3.81	4.64	3.71	4.89	3.17	4.31	5.14	5.29	7.47	6.71	7.79	8.29
Pulmonary acinus	10.32	5.25	9.04	3.50	9.55	5.86	13.27	2.14	7.08	1.37	7.05	1.08

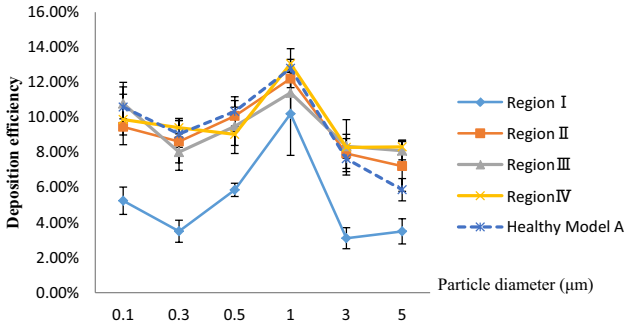

Fig. 9 Particle deposition results when alveoli become larger locally (Model E)

and showed that after alveolar volume expansion, the distance increased between the end of the airflow lines and the alveolar wall, which was not conducive to the diffusion deposition of particles and directly caused a decrease in the total deposition efficiency. Emphysema caused particle deposition to concentrate in the bronchus area, which would exacerbate bronchial obstruction, thereby causing further deterioration of emphysema lesions.

4.4 Impact of Particle Deposition in the Pulmonary Acinus on Inhalation Treatment

Chronic obstructive emphysema and pulmonary atrophy are common respiratory diseases. For example, in pneumoconiosis, current drug treatment mainly relieves the symptoms but cannot effectively remove lung dust. Lung lavage technology can effectively remove lung dust, but there are issues of high cost, patient suffering, more complications and other factors [27]. However, at present, the results of studies on the deposition of inhalable particles in the lung have shown that aerosol inhalation of soluble drugs is expected to provide an effective and more targeted clinical treatment method for chronic obstructive emphysema and other diseases. Previous reports [9] studied particle deposition after bronchiole obstruction and found that the deposition efficiencies of particles at the obstruction sites were significantly increased, while the deposition efficiencies in the alveoli were relatively reduced. The experimental model in this paper confirmed that the deposition efficiencies decreased after alveolar expansion. Regarding the clinical application significance, in bronchial obstructive emphysema, aerosol inhalation of drugs could target the drug to the obstruction site of the bronchus, but the drug could not reach the alveoli; therefore, drug release is safer and more effective. However, if the expansion is caused by alveolar lesions, as the deposition efficiency of the particle is very low, an ideal drug aerosol inhalation treatment effect cannot be achieved. Similarly, the deposition efficiencies of particles in atrophic

alveoli significantly increase, and the drug aerosol inhalation efficiency increases correspondingly. Therefore, the treatment is more targeted, and the drug efficiency is higher when drug aerosol inhalation treatment is selected.

5 Conclusion

Studies on the deposition patterns of particles in the pulmonary acinus have mainly focused on computer modeling analysis, but at present, the results of this analysis cannot be directly verified through in vivo experiments. In this study, by establishing a multiple-cluster pulmonary acinus in vitro experimental model, we analyzed particle deposition patterns in healthy, atrophic and expanded alveoli. The experimental results showed that the deposition efficiencies of particles in a healthy pulmonary acinus were relatively consistent with previous computer simulation results, and the deposition efficiency of particles with a 1 μm diameter was the highest. Alveolar morphology has a significant impact on particle deposition. Alveolar atrophy could increase the deposition efficiency of particles but did not have a significant impact on the deposition efficiency of the adjacent pulmonary acinus. Alveolar expansion could significantly decrease particle deposition efficiency, and in general, the particles concentrated in the pulmonary acinus and bronchus one level above. The testing results in this paper further confirmed previous theoretical analysis and computer simulation results of particle deposition in the pulmonary acinus. This model might provide a direct testing method for studies on particle deposition patterns in the pulmonary acinus in the presence of various human lesions and under various respiration modes. In addition, this study provides data in support of optimization of drug aerosol inhalation treatment for emphysema and other diseases.

Of course, this model has some limitations. The bronchioles and alveolar ducts of this model are composed of flexible material, but the deformation is very limited. In fact, the fine bronchioles and alveolar ducts in human lungs are more deformed when breathing. Therefore, this model cannot reproduce the effect of bronchoalveolar and alveolar duct deformation on the deposition of inhalable particles. In addition, the H number of this model is low when the particle diameter is more than 1 μm. Therefore, the influence of sedimentation deposition cannot be accurately simulated for large particles.

Acknowledgements This work was supported by the National Natural Science Foundation of China (Grant No. 31070832).

References

1. Tsuda, A., Henry, F. S., & Butler, J. P. (1995). Chaotic mixing of alveolated duct flow in rhythmically expanding pulmonary acinus. *Journal of Applied Physiology, 79*(3), 1055–1063.
2. Darquenne, C., Harrington, L., & Prisk, G. K. (2009). Alveolar duct expansion greatly enhances aerosol deposition: A three-dimensional computational fluid dynamics study. *Philosophical Transactions, 367*(1896), 2333–2346.
3. Sznitman, J., Heimsch, T., Wildhaber, J. H., Tsuda, A., & Rösgen, T. (2009). Respiratory flow phenomena and gravitational deposition in a three-dimensional space-filling model of the pulmonary acinar tree. *Journal of Biomechanical Engineering, 131*(3), 031010–031026.
4. Darquenne, C. (2014). Aerosol deposition in the human lung in reduced gravity. *Journal of Aerosol Medicine and Pulmonary Drug Delivery, 27*(3), 170–177.
5. Hofemeier, P., Koshiyama, K., Wada, S., & Sznitman, J. (2018). One (sub-)acinus for all: Fate of inhaled aerosols in heterogeneous pulmonary acinar structures. *European Journal of Pharmaceutical Sciences, 113*(15), 53–63.
6. Sznitman, J., Heimsch, F., Heimsch, T., Rusch, D., & Rösgen, T. (2007). Three-dimensional convective alveolar flow induced by rhythmic breathing motion of the pulmonary acinus. *Journal of Biomechanical Engineering, 129*(5), 658–665.
7. Ma, B., & Darquenne, C. (2011). Aerosol deposition characteristics in distal acinar airways under cyclic breathing conditions. *Journal of Applied Physiology, 110*(5), 1271–1282.
8. Oakes, J. M., Day, S., Weinstein, S. J., & Robinson, R. J. (2010). Flow field analysis in expanding healthy and emphysematous alveolar models using particle image velocimetry. *Journal of Biomechanical Engineering, 132*(2), 021008–021017.
9. Li, Z., Zhang, H., Cui, H., & Li, Y. (2016). Numerical simulation on characteristics of airflow and particles depositon in three-dimensional pulmonary acinus. *Chinese Journal of Applied Mechanics, 33*(5), 806–812.
10. Hofemeier, P., & Sznitman, J. (2016). The role of anisotropic expansion for pulmonary acinar aerosol deposition. *Journal of Biomechanics, 49*(14), 3543–3548.
11. Chhabra, S., & Prasad, A. K. (2010). Flow and particle dispersion in a pulmonary alveolus. Part 1. Velocity measurements and convective particle transport. *Journal of Biomechanical Engineering, 132*(5), 051009–051021.
12. Berg, E. J., Weisman, J. L., Oldham, M. J., & Robinson, R. J. (2010). Flow field analysis in a compliant acinus replica model using particle image velocimetry (PIV). *Journal of Biomechanics, 43*(6), 1039–1047.
13. Fishler, R., Mulligan, M. K., & Sznitman, J. (2013). Acinus-on-a-chip: A microfluidic platform for pulmonary acinar flows. *Journal of Biomechanics, 46*(16), 2817–2823.
14. Fishler, R., Hofemeier, P., Etzion, Y., Dubowski, Y., & Sznitman, J. (2015). Particle dynamics and deposition in true-scale pulmonary acinar models. *Scientific Reports, 5,* 14071–14082.
15. Fishler, R., Ostrovski, Y., Lu, C. Y., & Sznitman, J. (2017). Streamline crossing: An essential mechanism for aerosol dispersion in the pulmonary acinus. *Journal of Biomechanics, 50,* 222–227.
16. Listed, N. (1994). Human respiratory tract model for radiological protection. A report of a Task Group of the International Commission on Radiological Protection. *Annals of the Icrp, 24*(1–3), 1.

17. Haefeli-Bleuer, B., & Weibel, E. R. (1988). Morphometry of the human pulmonary acinus. *Anatomical Record Advances in Integrative Anatomy & Evolutionary Biology, 220*(4), 401–414.
18. Żywczyk, Ł., & Moskal, A. (2012). Modeling of the influence of tissue mechanical properties on the process of aerosol particles deposition in a model of human alveolus. *Journal of Drug Delivery Science & Technology, 22*(2), 153–159.
19. Sznitman, J. (2008). Respiratory flows in the pulmonary acinus and insights on the control of alveolar flows. *Paper presented at the International Conference on Sensors and Control Techniques* (ICSC2000).
20. Chen, J. H., Yuan, Z., Sheng, D. R., & Wei, L. I. (2012). Thermodynamic properties calculation method for moist air: 173 to 647 K. *Journal of Zhejiang University (Engineering Science Edition), 46*(4), 599–603.
21. Ding, Y. L., Cang, D. Q., & Yang, T. J. (1994). Concentration and viscosity of solid phase in a fully developed dilute gas-solid vertical flow. *Journal of University Offence & Technology Beijing*, *16*(1), 20–25.
22. Sznitman, J. (2013). Respiratory microflows in the pulmonary acinus. *Journal of Biomechanics, 46*(2), 284–298.
23. Hofemeier, P., & Sznitman, J. (2015). Revisiting pulmonary acinar particle transport: Convection, sedimentation, diffusion, and their interplay. *Journal of Applied Physiology, 118*(11), 1375–1385.
24. Oakes, J. M., Hofemeier, P., Vignonclementel, I. E., & Sznitman, J. (2015). Aerosols in healthy and emphysematous in silico pulmonary acinar rat models. *Journal of Biomechanics, 49*(11), 2213–2220.
25. Oakes, J. M., Marsden, A. L., Grandmont, C., Darquenne, C., & Vignon-Clementel, I. E. (2015). Distribution of aerosolized particles in healthy and emphysematous rat lungs: Comparison between experimental and numerical studies. *Journal of Biomechanics, 48*(6), 1147–1157.
26. Nai-Fang, F. U., Dong, Z. C., Xian-Jun, L. I., Chen, X. Q., Pan, R. H., Zheng, Y. Y., et al. (2016). Research progress on treatment methods of occupational pneumoconiosis. *Occupation & Health, 32*(24), 3452–3456.
27. Huang, C., & Respiration, D. O. (2016). Treatment and effect of chronic obstructive pulmonary emphysema. *China Continuing Medical Education, 4*(26), 105–106.